

See discussions, stats, and author profiles for this publication at: <https://www.researchgate.net/publication/339055530>

# Seasonal Shift From Biogenic to Geogenic Fluvial Carbon Caused by Changing Water Sources in the Wet- Dry Tropics

Article in *Journal of Geophysical Research: Biogeosciences* · February 2020

DOI: 10.1029/2019JG005384

CITATIONS

2

READS

260

9 authors, including:



**Clément Duvert**

Charles Darwin University

29 PUBLICATIONS 490 CITATIONS

[SEE PROFILE](#)



**Lindsay B. Hutley**

Charles Darwin University

232 PUBLICATIONS 7,709 CITATIONS

[SEE PROFILE](#)



**Christian Birkel**

University of Costa Rica

157 PUBLICATIONS 2,058 CITATIONS

[SEE PROFILE](#)



**Mitchel Rudge**

The University of Queensland

5 PUBLICATIONS 9 CITATIONS

[SEE PROFILE](#)

Some of the authors of this publication are also working on these related projects:



TROPISECA: Multi-lateral University Cooperation on the Management of Droughts in Tropical Catchments [View project](#)



The Antarctic Project [View project](#)

## JGR Biogeosciences

## RESEARCH ARTICLE

10.1029/2019JG005384

## Key Points:

- Seasonal changes in hydrological connectivity control the sources and fluxes of inorganic carbon
- Under wet conditions, most inorganic carbon is biogenic and transported by surface and subsurface flow paths
- Under dry conditions, most inorganic carbon is geogenic and transported by older, deeper flow paths

## Supporting Information:

- Supporting Information S1

## Correspondence to:

C. Duvert,  
clem.duvert@cdu.edu.au










## Citation:

Duvert, C., Hutley, L. B., Birkel, C., Rudge, M., Munksgaard, N. C., Wynn, J. G., et al. (2020). Seasonal shift from biogenic to geogenic fluvial carbon caused by changing water sources in the wet-dry tropics. *Journal of Geophysical Research: Biogeosciences*, 125, e2019JG005384. <https://doi.org/10.1029/2019JG005384>

Received 18 JUL 2019

Accepted 6 NOV 2019

## Seasonal Shift From Biogenic to Geogenic Fluvial Carbon Caused by Changing Water Sources in the Wet-Dry Tropics

Clément Duvert<sup>1</sup> , Lindsay B. Hutley<sup>1</sup> , Christian Birkel<sup>2,3</sup> , Mitchel Rudge<sup>4</sup> , Niels C. Munksgaard<sup>5</sup> , Jonathan G. Wynn<sup>6</sup> , Samantha A. Setterfield<sup>7</sup> , Dioni I. Cendón<sup>8</sup> , and Michael I. Bird<sup>5</sup> 

<sup>1</sup>Research Institute for the Environment and Livelihoods, Charles Darwin University, Darwin, Northern Territory, Australia, <sup>2</sup>Department of Geography and Water and Global Change Observatory, University of Costa Rica, San José, Costa Rica, <sup>3</sup>Northern Rivers Institute, University of Aberdeen, Aberdeen, Scotland, <sup>4</sup>Sustainable Minerals Institute, University of Queensland, Brisbane, Queensland, Australia, <sup>5</sup>College of Science and Engineering, James Cook University, Cairns, Queensland, Australia, <sup>6</sup>National Science Foundation, Alexandria, VA, USA, <sup>7</sup>School of Biological Sciences, The University of Western Australia, Perth, Western Australia, Australia, <sup>8</sup>Australian Nuclear Science and Technology Organisation, Sydney, New South Wales, Australia

**Abstract** The riverine export of carbon is expected to be driven by changes in connectivity between source areas and streams. Yet we lack a thorough understanding of the relative contributions of different water sources to the dissolved carbon flux, and of the way these contributions vary with seasonal changes in flow connectivity. Here we assess the temporal variations in water and associated dissolved inorganic carbon (DIC) sources and fluxes in a wet-dry tropical river of northern Australia over two years. We use linear mixing models integrated into a Bayesian framework to determine the relative contributions of rainfall, seasonal wetlands, shallow groundwater, and a deep carbonate aquifer to riverine DIC fluxes, which we relate to the age of water sources. Our results suggest extreme shifts in water and DIC sources between the wet and dry seasons. Under wet conditions, most DIC was of biogenic origin and transported by relatively young water sources originating from shallow groundwater and wetlands. As rainfall ceased, the wetlands either dried out or became disconnected from the stream network. From this stage, DIC switched to a geogenic origin, nearly entirely conveyed via older water sources from the carbonate formation. Our findings demonstrate the importance of changing patterns of connectivity when evaluating riverine DIC export from catchments. This work also illustrates the need to systematically partition DIC fluxes between biogenic and geogenic sources, if we are to quantify how the riverine export of carbon affects net carbon soil storage.

### 1. Introduction

There is now consensus that tropical regions are hot spots of fluvial carbon (C) export (e.g., Borges et al., 2015; Mann et al., 2014; Sawakuchi et al., 2017). The wet-dry (or seasonal) tropics cover >60% of the global tropics (Peel et al., 2007), yet the dynamics and magnitude of fluvial C export in this bioclimatic zone have received far less attention than those in the humid tropics. Recent evidence suggests above-average rates of dissolved inorganic carbon (DIC) export in streams and rivers of the wet-dry tropics (Tweed et al., 2016; Duvert, Bossa, et al., 2019), a finding that emphasizes the need for further research to better constrain both regional and global C budgets.

Extreme seasonality in rainfall and primary production, a distinctive feature of the wet-dry tropics, results in concurrent increases in water and C inputs to catchments over relatively short periods of time (days to months). By enabling direct connectivity between source areas and stream networks and by increasing stream transport capacity, wet conditions are likely to generate high rates of DIC export to rivers. Conversely, during the extended dry season(s), entire portions of the landscape can become disconnected from river networks, at least superficially. These marked seasonal changes in hydrological connectivity translate into changes in the dominant flow paths to rivers, which in turn can result in significant shifts in DIC sources. For instance, high riverine DIC concentrations have been linked to enhanced connectivity with seasonal floodplains (Geeraert et al., 2017) and with the shallow subsurface (Tweed et al., 2016) under wet conditions. In contrast, where DIC originates from deeper groundwater, baseflow conditions can result in higher

riverine DIC concentrations (Mann et al., 2014; Shih et al., 2018). Because different water flow paths can carry DIC of different origins (Oviedo-Vargas et al., 2015), understanding the DIC export dynamics in rivers of the wet-dry tropics requires an assessment of both water and DIC sources and pathways.

Prior research has extensively investigated the sources and pathways of dissolved organic C (DOC) to streams and rivers (e.g., Boyer et al., 1997; Fiebig et al., 1990; Laudon et al., 2011), laying the foundations for approaches that now integrate water and DOC tracing methods (Birkel et al., 2017; Dick et al., 2015; Tunaley et al., 2016; Zimmer & McGlynn, 2018). In comparison, the dynamics of DIC across catchments have only gained interest more recently, with a predominance of studies from northern Europe (e.g., Campeau et al., 2017; Campeau et al., 2018; Öquist et al., 2009; Waldron et al., 2007; Wallin et al., 2010). Fewer studies have been conducted in tropical streams and rivers, although DIC may represent a larger export flux than DOC in the tropics (Huang et al., 2012). In these regions, questions remain regarding the role of hydrological connectivity and dominant flow paths in controlling DIC mobilization and transport, as well as the partitioning between these sources.

The current shortfall in our understanding of fluvial DIC dynamics largely stems from the inherent difficulty of examining this flux. Unlike DOC, DIC can easily convert into different carbonate species ( $\text{CO}_2^*$ ,  $\text{HCO}_3^-$ ,  $\text{CO}_3^{2-}$ ) who are semiconservative in sum, although the relative concentrations of the constituent species will change as a function of pH. DIC can also originate from a wide range of sources within catchments. Seasonally inundated wetlands associated with tropical rivers are increasingly seen as a key landscape unit for the production of biogenic DIC and subsequent export via connected river systems (Abril & Borges, 2019; Borges et al., 2015; Geeraert et al., 2017; Teodoru et al., 2015). Subsurface flow and shallow groundwater are also potential conveyors of biogenic DIC, with  $p\text{CO}_2$  within those components often  $>50,000$  ppm in the tropics (Johnson et al., 2008; Duvert et al., 2018; Duvert, Bossa, et al., 2019). Biogenic DIC can also be produced internally, with aquatic metabolism releasing  $\text{CO}_2$  into the water column (Waldron et al., 2007). Finally, where soils contain pedogenic carbonates or are underlain by carbonate rocks, the weathering of soil or parent geological material can contribute geogenic DIC to rivers via groundwater flow paths (Shin et al., 2011; Telmer & Veizer, 1999; Violette et al., 2010). Despite this complexity, knowledge of the origin of fluvial DIC is critical, not only to refine our understanding of C transport through catchments but also to determine what proportion of the DIC flux will contribute to a loss of soil C storage.

The stable isotopic signature of DIC ( $\delta^{13}\text{C}_{\text{DIC}}$ ) is often used to distinguish between different DIC sources (Campeau et al., 2017). Biogenic and geogenic sources have a dissimilar  $\delta^{13}\text{C}_{\text{DIC}}$  signature, especially in the wet-dry tropics where vegetation is typically a C3-C4 mixture relatively depleted in  $^{13}\text{C}$ , whereas DIC originating from rock weathering will have a more enriched signature. Despite its usefulness as a tracer of DIC origin,  $\delta^{13}\text{C}_{\text{DIC}}$  can also be affected by a range of external and in-stream processes that alter its original signature (see discussion in Campeau et al. (2018)). In this context, the use of multiple tracers with contrasting characteristics can help reduce uncertainties in the quantification of different sources (Abbott et al., 2016). Water source partitioning techniques using electrical conductivity (EC) or silica have proven particularly useful in deciphering the role of hydrological flow paths in delivering  $\text{CO}_2$  and DIC to streams (Horgby et al., 2019; Johnson et al., 2007; Winterdahl et al., 2016).

In this paper, we use DIC concentrations and  $\delta^{13}\text{C}_{\text{DIC}}$  to assess the sources and fluxes of DIC to a wet-dry tropical river of northern Australia over two years. We also estimate the seasonal changes in dominant water sources and hydrological connectivity using tritium, water stable isotopes, and EC. Using this knowledge, we quantify mass fluxes of biogenic versus geogenic DIC to the river. We test the hypotheses that (1) the marked seasonal cycle of rainfall in the region will drive changes in dominant flow paths and hydrological connectivity between wetlands, aquifers, and rivers and (2) these hydrological changes will result in shifting sources of DIC to rivers.

## 2. Data and Methods

### 2.1. Site Description

The Howard River catchment (126 km<sup>2</sup>) is located 30 km east of Darwin, in the wet-dry tropics of northern Australia (Figure 1). It is a lowland area dominated by tropical savanna with wetlands and seasonally inundated floodplains. Over 90% of rainfall occurs between November and April. The median annual rainfall for

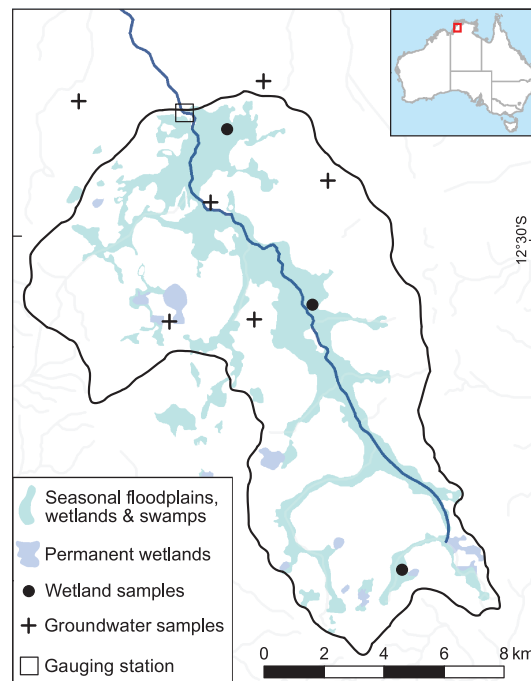


**Figure 1.** Location of the Howard River catchment in the wet-dry tropics of Australia (Northern Territory). The black line corresponds to the catchment boundaries. The areas covered by seasonal and permanent wetlands were mapped based on land, soil, and vegetation mapping products by the Northern Territory Government.

years 1986–2016 was 1,879 mm/year (Bureau of Meteorology rain gauge at Howard Springs; range 1,335–2,881 mm/year). The geology consists of a shallow lateritic profile (1–3 m) that contains a network of connected solution cavities (Doyle, 2001), with potential implications for subsurface water movement. This weathering layer is underlain by a heterogeneous sandstone/claystone formation (depth 10–40 m), which contains a shallow aquifer (Doyle, 2001). About 10% of annual rainfall contributes to recharging this aquifer, most of which then enters the river as baseflow (Cook et al., 1998). At the base of the sandstone is a layer of unconsolidated sand, which overlies a highly weathered dolostone formation (Doyle, 2001), the Koolpinyah Dolomite, a major aquifer in the Darwin area used extensively for agriculture and domestic water supplies.

At the peak of the wet season, seasonal wetlands and inundated land occupy about 23% of the catchment area (Figure 1; Duvert, Bossa, et al., 2019). River flow then slowly recedes and the upstream part of the surface network usually dries out by around July. Duvert, Bossa, et al. (2019) investigated the spatial variations in  $\delta^{13}\text{C}_{\text{DIC}}$  along the river during flow recession. Water sourced from the shallow groundwater and seasonal wetlands had a strong effect on the hydrology of the upstream part of the catchment, with  $\delta^{13}\text{C}_{\text{DIC}}$  around  $-20.7 \pm 3.1\text{‰}$ , whereas the dolomite aquifer contributed more water and geogenic DIC to the downstream sections of the river, with  $\delta^{13}\text{C}_{\text{DIC}}$  values of  $-15.8 \pm 0.1\text{‰}$  (Duvert, Bossa, et al., 2019). These results indicated important spatial variations in water and DIC sources along the river.

## 2.2. Sample Collection and Laboratory Analyses

Over a two-year period, 75 river samples were collected at the Howard River gauging station (Northern Territory Government; G8150179) for determination of DIC,  $\delta^{13}\text{C}_{\text{DIC}}$ , and water stable isotopes ( $\delta\text{D}$  and  $\delta^{18}\text{O}$ ). Samples were collected from January 2017 until February 2019 on a weekly (during high flow) to monthly (during baseflow) basis. For each sampling date, EC, pH, and water temperature were obtained from a set of automated sensors (Campbell Scientific, USA) connected to a logger on site. Before sampling, bottles were rinsed thoroughly 3 times and samples were collected by immersing the bottle about 20 cm below the water surface.

To characterize the different water and DIC sources potentially feeding the river, we used the groundwater data from Duvert, Bossa, et al. (2019) and Rudge (2015) for both the shallow (sampled at 2–18 m below the surface) and deep (sampled at 21–36 m below the surface) aquifers. We supplemented these data with samples collected from three seasonal wetlands located within the catchment boundaries (Figure 1) in June 2017 and May 2018, and with two rainfall samples collected in January and March 2018. Values of DIC,  $\delta^{13}\text{C}_{\text{DIC}}$ ,  $\delta\text{D}$ , and  $\delta^{18}\text{O}$  were determined for all these samples. In addition, for a subset of source samples, the partial pressure of  $\text{CO}_2$  ( $p\text{CO}_2$ ) was measured directly in the water using an eosGP sensor (Eosense, Canada), calibrated using 0-, 5,000-, and 10,000-ppm Calgaz standards.

Six river samples were collected in 2017 for determination of tritium ( $^3\text{H}$ ). Two rainfall samples as well as one sample representative of each groundwater system (shallow sandstone and deep dolostone) were also collected for  $^3\text{H}$  analysis. Lastly, we used long-term  $^3\text{H}$  rainfall time series, collected monthly at Darwin airport and analyzed by the Australian Nuclear Science and Technology Organisation from 1963 to 2017. We also used a daily data set of  $\delta\text{D}$  and  $\delta^{18}\text{O}$  in rainfall collected in Darwin ( $n = 349$ ; period 2014–2018; Munksgaard and Lambrinidis, unpublished data) to derive a local meteoric water line (see Figure S1 in the supporting information).

All samples were kept refrigerated and in dark until they were analyzed at Charles Darwin University (Environmental Chemistry and Microbiology Unit). DIC and  $\delta^{13}\text{C}_{\text{DIC}}$  were measured with an ISO-CADICA instrument, which consists of an extraction chamber connected to a Picarro G2101-i cavity ring-down spectrometer (Bass et al., 2012). All  $\delta^{13}\text{C}_{\text{DIC}}$  values are reported as per mil deviations from the standard Vienna Pee Dee Belemnite. According to replicate analyses, analytical precision ( $\pm\sigma$ ) was  $\pm 0.54\%$  for  $\delta^{13}\text{C}_{\text{DIC}}$  and  $\pm 0.49 \text{ mg L}^{-1}$  for DIC. Oxygen-18 ( $\delta^{18}\text{O}$ ) and  $\delta\text{D}$  were analyzed using a Picarro L2130-i cavity ring-down spectrometer fitted with a diffusion sampler (Munksgaard et al., 2011). The data were calibrated to Vienna Standard Mean Ocean Water by analysis of three standard waters of known isotopic composition. According to replicate analyses, analytical precision ( $\pm\sigma$ ) was  $\pm 0.02\%$  for  $\delta^{18}\text{O}$  and  $\pm 0.23\%$  for  $\delta\text{D}$ .

All 10  $^3\text{H}$  samples were analyzed at the Australian Nuclear Science and Technology Organisation in Sydney. Samples were distilled and electrolytically enriched between 67- and 70-fold prior to counting with a liquid scintillation counter for several weeks. The limit of quantification was 0.07 tritium units (TU) for all samples, and analytical precision was between  $\pm 0.03$  and  $\pm 0.06$  TU. All data used in this study are available in the Hydroshare repository (Duvert, Alvarez, et al., 2019).

### 2.3. Data Analyses

#### 2.3.1. Source Water Age Estimates

To discriminate water sources, and particularly the deep groundwater from wetland contributions, we estimated source water ages based on streamwater  $^3\text{H}$  data. We followed a methodology similar to that described in Duvert et al. (2016), whereby an input function was derived from monthly  $^3\text{H}$  measurements in Darwin rainfall (1963–2017). All the months with  $P < 50$  mm were discarded from the data set as  $^3\text{H}$  measurements were not always available for those months, and, more importantly, rainfall during those intermediate months (typically September to November) was less likely to contribute to recharge. We extended the input data set for the period 1900–1962 with a constant value corresponding to the average of  $^3\text{H}$  activity between 2014 and 2018, that is, 1.04 TU ( $n = 26$ ). The reasoning here is that in the southern hemisphere, the atmospheric  $^3\text{H}$  activity has now declined back to prebomb levels (Stewart & Morgenstern, 2016). We then adjusted a time-invariant age distribution function ( $g$ ) to this input function ( $C_{\text{in}}$ ) and our river output  $^3\text{H}$  measurements ( $C_{\text{out}}$ ), using a convolution integral weighted by precipitation (Małozewski & Zuber, 1982; Stewart & McDonnell, 1991):

$$C_{\text{out}}(t) = \frac{\int_0^{\infty} C_{\text{in}}(t-t_e) P(t-t_e) e^{-\lambda t_e} g(t_e) dt_e}{\int_0^{\infty} P(t-t_e) g(t_e) dt_e}$$

where  $t_e$  is time of entry in the catchment,  $e^{-\lambda t_e}$  is a decay term that accounts for  $^3\text{H}$  decay once in the ground ( $\lambda = 1.54 \times 10^{-4} \text{ days}^{-1}$ ), and  $P$  is the monthly precipitation. We used a Gamma model as an age distribution function, as this is known to represent catchment functioning more accurately (Kirchner et al., 2000). To determine the best fit parameters  $\alpha$  and  $\beta$ , we ran 10,000 simulations with randomized values in the range

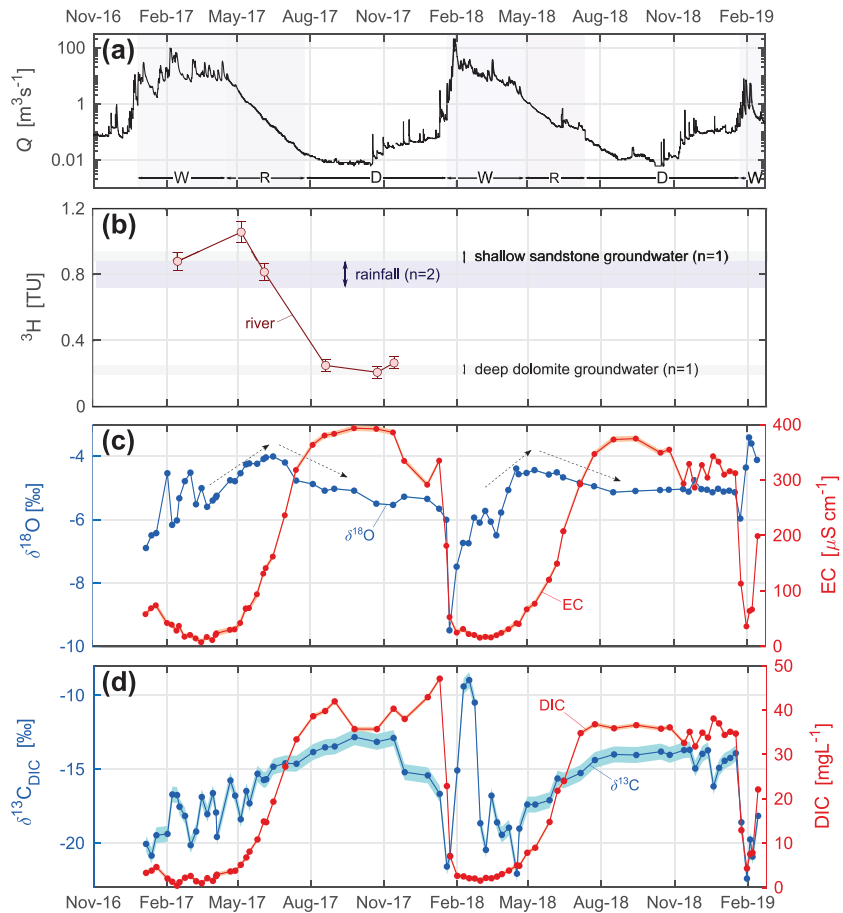


**Figure 2.** Time series of (a) discharge, (b)  $^3\text{H}$ , (c)  $\delta^{18}\text{O}$  and EC (“water tracers”), and (d)  $\delta^{13}\text{C}_{\text{DIC}}$  and DIC (“carbon tracers”) in the Howard River. In (a), “W,” “R,” and “D” stand for wet, recession, and dry seasons, respectively. Arrows in (c) symbolize a seasonal turning point from increasingly evaporated waters originating from wetland drainage to more depleted waters representative of the deep aquifer. For all tracers, shaded areas and error bars correspond to 2 standard deviations based on replicate measurements.

[0–4] for  $\alpha$  and [100–5,000] for  $\beta$ . Each realization was assessed by calculating the absolute error between the model outputs and our measured  $C_{\text{out}}$  values. We adjusted a gamma function for the samples collected under high-flow conditions ( $n = 3$ ) and also for the samples collected during the dry season ( $n = 3$ ). Data processing and analyses for the water age estimates were performed using MATLAB R2017b.

### 2.3.2. Bayesian Source Water Mixing Models

We used linear mixing models implemented in a Bayesian framework to distinguish between different water and DIC contributions to the river. The R package MixSIAR (Stock & Semmens, 2016) was used for this purpose. For a detailed description of the theory underlying these models, the reader is referred to Parnell et al. (2013). To determine the water source proportions in river water, we performed mixing analyses using  $\delta^{18}\text{O}$  and EC, both these tracers being commonly used in source partitioning analyses. To determine the DIC proportions in river water, we performed mixing analyses using  $\delta^{13}\text{C}_{\text{DIC}}$  and DIC. The source end-members considered for each analysis were (i) rainfall ( $n = 2$ ), (ii) seasonal wetlands ( $n = 3$ ), (iii) shallow sandstone aquifer ( $n = 18$ ), and (iv) deep dolomite aquifer ( $n = 10$ ). For rainfall, the end-member values (mean and standard deviation) for  $\delta^{18}\text{O}$  were calculated from 349 values collected in Darwin between 2014 and 2018.

Similar to our approach for the streamwater age estimates, we separated the tracer time series into three periods according to the following rules: the “wet” period started when cumulative rainfall for the previous 10 days ( $P_{10\text{d}}$ ) was  $>100$  mm, the “recession” period started when  $P_{10\text{d}}$  was  $<10$  mm, and the “dry” period started when flow rate decreased below a  $0.05\text{-m}^3 \text{ s}^{-1}$  threshold. Over the two-year survey, we collected

33, 16, and 26 samples during the wet, recession, and dry periods, respectively. Of the 75 river samples, 22 of them had no EC data. We gap filled the EC time series with a multiple linear regression, using DIC and discharge as predictor variables ( $R^2 = 0.95$ ). Data processing and analyses for the mixing model calculations were performed using R version 3.5.1 (R Core Team, 2018).

We note that a range of physical and biogeochemical processes can potentially affect the  $\delta^{13}\text{C}_{\text{DIC}}$  signature of river waters, including  $\text{CO}_2$  evasion (Doctor et al., 2008) and in-stream photosynthesis (Parker et al., 2005). The omission of these factors in our models may have generated inaccuracies in some of the mixing results. In section 4, we further address the uncertainties that are likely to stem from these in-stream processes.

### 2.3.3. DIC Source and Flux Calculations

Under the assumption that for each of the three periods (wet, recession, and dry), a single source of DIC contributed to the riverine DIC load, we evaluated the isotopic signature of this source using Keeling (Keeling, 1958) and Miller-Tans (Miller & Tans, 2003) plots based on river samples, following the methodology described in Campeau et al. (2017) and Campeau et al. (2018). Prior to plotting, we removed outliers from each data set, that is, all  $\delta^{13}\text{C}_{\text{DIC}}$  values greater than three scaled median absolute deviations away from the median. There were three outliers in the wet season data and two outliers in the dry season data.

To distinguish the biogenic versus geogenic DIC contributions to streamflow for each of the three previously established periods, we first calculated the mean river discharge per period based on high-frequency discharge records at the Howard River gauging station. Using the relative source contributions obtained from the Bayesian source mixing analyses, we then defined the fraction of discharge delivered by each source. These fractions of water flux were multiplied by the average DIC concentration in each source to derive a DIC flux per source and per period. We also multiplied each water flux by the average  $\text{CO}_2$  concentration in each source to determine the fraction of DIC contributed by  $\text{CO}_2$ . Given the  $\delta^{13}\text{C}_{\text{DIC}}$  data measured in each source, we assumed that all DIC originating from shallow groundwater and wetlands was of biogenic origin, whereas the DIC originating from the deep aquifer was of equivalent proportions of biogenic (50%) and geogenic (50%) origins. The latter is because we consider that  $\text{CO}_2$  from respiration drives chemical weathering; hence, one mole of biogenic C is needed to dissolve one mole of geogenic C (e.g., Telmer & Veizer, 1999). This weathering reaction is likely enabled by long water residence time within the aquifer and the rapid kinetics of carbonate dissolution. Lastly, we assumed that rainfall carried negligible amounts of DIC.

## 3. Results

### 3.1. Flow Regime and Hydrological Connectivity

According to three Bureau of Meteorology rain gauges located within the catchment (Howard Springs, McMinns Lagoon, and Girraween), rainfall was well above average during the water year 2016–2017 (September to August; 2,450 mm), above average in 2017–2018 (2,030 mm), and well below average in 2018–2019 (1,270 mm). Most rain fell between December and March, resulting in pronounced seasonal oscillation in streamflow data (Figure 2a). Mean daily discharge varied between  $6 \times 10^{-3}$  and  $144 \text{ m}^3 \text{ s}^{-1}$  over the course of the study. The highest-flow event occurred in late January 2018 when instantaneous peak discharge reached  $207 \text{ m}^3 \text{ s}^{-1}$ , an event with an eight-year return period (Galton frequency analysis). Mean daily baseflow was between  $6 \times 10^{-3}$  and  $3 \times 10^{-2} \text{ m}^3 \text{ s}^{-1}$  and high flow between 1 and  $144 \text{ m}^3 \text{ s}^{-1}$ .

### 3.2. Source Water Age Estimates

Tritium values in streamwater decreased considerably from wet to dry conditions (Figure 2d). The two samples collected at high flow (0.88 and 1.06 TU) and the sample collected during flow recession (0.81 TU) were within the same range as current rainfall input  $^3\text{H}$  activity ( $1.04 \pm 0.23$  TU; 0.86 and 0.73 TU for our two 2018 rainfall samples) and similar to waters from the shallow aquifer (0.90 TU). The three low flow samples were much more depleted in  $^3\text{H}$  ( $0.25 \pm 0.03$  TU), comparable to the  $^3\text{H}$  activity measured in the deeper aquifer (0.24 TU). The gamma age distribution adjusted to the three high-flow samples returned a mean streamwater age of  $7 \pm 3$  months ( $\alpha$  [0–0.08] and  $\beta$  [500–814]). For the low-flow component, our simulations suggest that the older flow component had a mean age older than 100 years. However, we were unable to determine an accurate age distribution due to the very low  $^3\text{H}$  activity in the river for these low-flow samples.

### 3.3. Water Stable Isotopes, EC, DIC, and $\delta^{13}\text{C}_{\text{DIC}}$

All tracers varied substantially between wet and dry conditions (Figure 2). Our local meteoric water line yielded  $\delta\text{D} = 7.8 \delta^{18}\text{O} + 13.2$  (Figure S1), similar to the long-term equation reported by Hollins et al. (2018) for Darwin ( $\delta\text{D} = 7.82 \delta^{18}\text{O} + 10.27$ ). Due to large short-term variations in rainfall isotopic signature,  $\delta\text{D}$  and  $\delta^{18}\text{O}$  in the river tended to be much more variable during the wet season, with values alternatively enriched and depleted ( $\delta^{18}\text{O}$  between  $-9.5$  and  $-3.4\text{‰}$ , median  $-5.7\text{‰}$ ; Figure 2b). In particular, the rainfall events at the onset of the wet season were always highly depleted, resulting in a decrease in river isotopic values. In contrast, values during flow recession and the dry season followed a more gradual trend, first with increasing (median and standard deviation  $-4.4 \pm 0.3\text{‰}$ ) then decreasing isotopic ratios ( $-5.1 \pm 0.2\text{‰}$ ; arrows in Figure 2b). Wetlands were in general more enriched in  $^{18}\text{O}$  ( $-3.0 \pm 2.0\text{‰}$ ), reflecting evaporative enrichment in these stagnant waters (as also confirmed by lower deuterium excess values), whereas values in the two groundwater bodies were more depleted ( $-6.4 \pm 0.6\text{‰}$  and  $-5.7 \pm 1.1\text{‰}$  for the shallow and deep aquifer, respectively).

River water DIC and EC values varied similarly. They were higher during the dry season ( $35.9 \pm 3.4 \text{ mg L}^{-1}$  and  $336 \pm 36 \mu\text{S cm}^{-1}$ ) and were affected by rainwater dilution during the wet season ( $2.5 \pm 4.2 \text{ mg L}^{-1}$  and  $23 \pm 37 \mu\text{S cm}^{-1}$ ; Figures 2b and 2c), with a gradual increase during flow recession for both parameters ( $12.8 \pm 7.7 \text{ mg L}^{-1}$  and  $109 \pm 69 \mu\text{S cm}^{-1}$ ). The riverine DIC concentrations and EC values during the dry season reflected values from the deep aquifer ( $41.6 \pm 9.8 \text{ mg L}^{-1}$  and  $257 \pm 135 \mu\text{S cm}^{-1}$ ) and to a lesser extent from the shallow aquifer ( $25.8 \pm 11.1 \text{ mg L}^{-1}$  and  $34 \pm 17 \mu\text{S cm}^{-1}$ ), while values measured during the wet season were more similar to wetland waters ( $3.0 \pm 0.2 \text{ mg L}^{-1}$  and  $35 \pm 16 \mu\text{S cm}^{-1}$ ) and rainfall ( $<0.05 \text{ mg L}^{-1}$  and  $17 \pm 1 \mu\text{S cm}^{-1}$ ).

The time series of  $\delta^{13}\text{C}_{\text{DIC}}$  also varied markedly with flow conditions, with generally more  $^{13}\text{C}$ -depleted signatures during the wet season ( $-19.0 \pm 3.2\text{‰}$ ), and more enriched at baseflow ( $-14.0 \pm 0.9\text{‰}$ ; Figure 2c). However, there were also occurrences of high  $\delta^{13}\text{C}_{\text{DIC}}$  during the wet season, such as February 2018 during a major runoff event ( $-9.9 \pm 2.8\text{‰}$ ;  $n = 4$ ; Figure 2c). Looking at end-members, the most  $^{13}\text{C}$ -depleted waters were from the shallow groundwater ( $-26.6 \pm 1.3\text{‰}$ ), while wetlands also had low  $\delta^{13}\text{C}_{\text{DIC}}$  ( $-23.1 \pm 2.5\text{‰}$ ), both typical of biogenic C and reflecting a dominance of the C3 photosynthetic pathway in the savanna C3-C4 mixture. Carbon isotopic ratios in the deep aquifer were more enriched and likely due to a mixture of both biogenic and geogenic sources ( $-15.5 \pm 2.7\text{‰}$ ). In comparison, the  $\delta^{13}\text{C}$  of the dolostone itself was  $-3.4 \pm 0.8\text{‰}$  ( $n = 6$ ; Rudge, 2015). Rainfall had  $^{13}\text{C}$ -enriched signatures, with values around  $-7.8 \pm 1.1\text{‰}$ .

Upon initial inspection, the DIC and  $\delta^{13}\text{C}_{\text{DIC}}$  data pairs for river samples plotted close to the deep groundwater end-member during the dry season (low flow), and between wetland drainage, rainfall, and to a lesser extent near shallow groundwater end-members during the wet season (Figure 3a). A similar pattern can be observed for the EC and  $\delta^{18}\text{O}$  data pairs, with baseflow samples clustering around the deep groundwater, whereas high flow and recession samples were scattered between all four end-members (Figure 3b).

### 3.4. Seasonal Variations in DIC Sources

Results obtained from the Miller-Tans and Keeling linear mixing models suggest that the sources of DIC to the river during the wet season were more  $^{13}\text{C}$ -depleted than during recession, and much more  $^{13}\text{C}$ -depleted than during the dry season (Table 1). The source estimates for the wet season resemble  $\delta^{13}\text{C}_{\text{DIC}}$  signatures measured in wetlands, while the much more  $^{13}\text{C}$ -enriched source estimates for the dry season are closer to the  $\delta^{13}\text{C}_{\text{DIC}}$  signatures measured in the dolostone aquifer.

### 3.5. Bayesian Source Water Mixing Analysis

The Bayesian mixing analyses yielded contrasting results for each flow period (Figure 4). According to the analysis based on water tracers ( $\delta^{18}\text{O}$  and EC),  $63 \pm 14\%$  of water originated from the shallow groundwater during the wet season, with rainfall and wetland contributing the remaining water flux ( $18 \pm 12\%$  and  $11 \pm 13\%$ , respectively; Figure 4a). The analysis yielded more uncertain results for the flow recession period, with all sources contributing between 11% (shallow groundwater) and 32% (wetland; Figure 4b). The dry season had an overwhelming contribution from the deep dolostone aquifer ( $89 \pm 5\%$ ) while the three other sources accounted for  $<4\%$  each (Figure 4c).



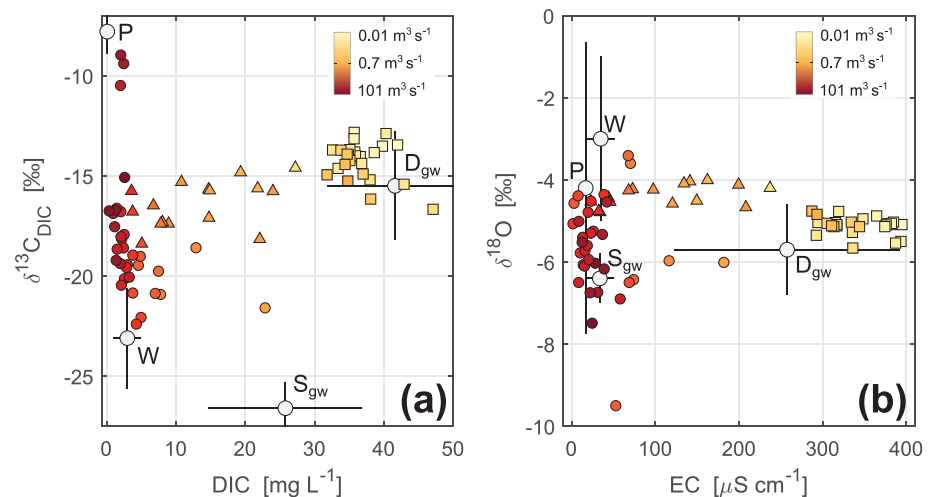


**Figure 3.** Variations in DIC,  $\delta^{13}\text{C}_{\text{DIC}}$ , EC, and  $\delta^{18}\text{O}$  in the Howard River and four identified end-members. (a) Dual plot of DIC versus  $\delta^{13}\text{C}_{\text{DIC}}$ . (b) Dual plot of EC versus  $\delta^{18}\text{O}$ . P is precipitation ( $n = 2$ ), W is wetland drainage ( $n = 3$ ),  $S_{\text{gw}}$  is shallow sandstone groundwater ( $n = 18$ ), and  $D_{\text{gw}}$  is deep dolomite groundwater ( $n = 10$ ). The color of each marker corresponds to its associated discharge value. Circles, triangles, and squares are for samples taken during the wet season, recession, and dry season, respectively. The range for each end-member corresponds to 2 standard deviations.

According to the mixing analysis for C source proportions (using  $\delta^{13}\text{C}_{\text{DIC}}$  and DIC as tracers), during the wet season the bulk of DIC originated from the drainage of seasonal wetlands and floodplains ( $61 \pm 8\%$ ) and from rainfall, that is, direct runoff ( $32 \pm 7\%$ ; Figure 4d). During the few months of flow recession, the analysis suggested mixed contributions from the four sources, with a slight prevalence of rainfall ( $40 \pm 8\%$ ) and a more limited input from the deep aquifer ( $17 \pm 9\%$ ; Figure 4e). Lastly under low-flow conditions, the DIC source proportions were equivalent to our results for water sources, with the deep aquifer dominating the overall flux ( $82 \pm 6\%$ ; Figure 4f).

### 3.6. Biogenic Versus Geogenic Flux Estimates

Flux estimates differed depending on which variables were used for source contributions in the Bayesian mixing model (Table 2). Estimates based on water tracer partitioning ( $\delta^{18}\text{O}$  and EC) yielded a much larger DIC flux ( $20.6 \text{ Mg C km}^{-2} \text{ yr}^{-1}$ ) than those based on C tracer partitioning ( $\delta^{13}\text{C}_{\text{DIC}}$  and DIC;  $5.4 \text{ Mg C km}^{-2} \text{ yr}^{-1}$ ). According to both source mixing scenarios, the biogenic flux ( $19.3$  and  $4.5 \text{ Mg C km}^{-2} \text{ yr}^{-1}$ , respectively) was greater than the geogenic flux ( $1.3$  and  $0.9 \text{ Mg C km}^{-2} \text{ yr}^{-1}$ , respectively), with the former accounting for 83–94% of the total DIC flux. The difference between flux estimates between models can be explained by the differences in source contributions (Figure 4): according to the first Bayesian analysis (water tracers) the  $\text{CO}_2$ -rich shallow groundwater contributed the bulk of streamflow in the wet season, whereas in the second Bayesian analysis (C tracers) most of wet season DIC originated from the wetlands, characterized by much lower average DIC concentrations.

**Table 1**  
Isotopic Compositions of the Main DIC Source (%) Per Season as Obtained From the Miller-Tans and Keeling Plots After Removing Outliers

	Keeling	Miller-Tans
Wet	−19.9	−21.2
Recession	−15.9*	−15.3
Dry	−12.1*	−11.8

Note. All Miller-Tans regressions were significant ( $p < 0.001$ ) while two Keeling regressions were not significant ( $p > 0.005$ ; marked with asterisk in the table).

For both source mixing scenarios, dissolved  $\text{CO}_2$  contributed about 70% to biogenic DIC, and only about 10% to geogenic C. Seasonally, the DIC flux was almost entirely biogenic during the wet season when flow rate was highest, while it was a mixture of biogenic and geogenic during flow recession, and purely geogenic during the dry season (Table 2)—although under our assumption that biogenic C is needed to initiate chemical weathering, the dry season flux was actually made up of equivalent proportions of geogenic and biogenic C. Interestingly, the geogenic C flux was highest, but diluted by other sources, during the wet season, and lowest, but relatively undiluted, during the dry season.

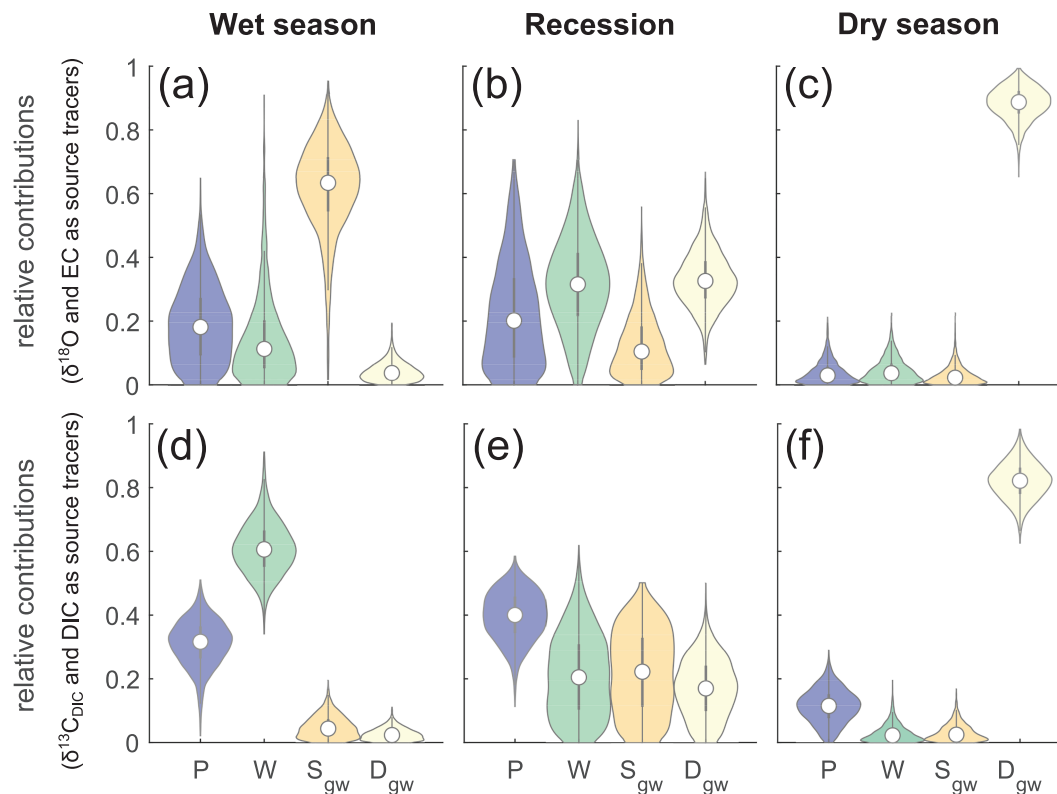


**Figure 4.** Relative contributions of four sources to the water and DIC riverine fluxes. (a–c) The violin plots were obtained using  $\delta^{18}\text{O}$  and EC as source tracers. (d–f) The plots were obtained using  $\delta^{13}\text{C}_{\text{DIC}}$  and DIC as source tracers. (a) and (d) correspond to results for the wet season samples, (b) and (e) for flow recession, and (c) and (f) for the dry season. P is precipitation, W is wetland drainage,  $S_{\text{gw}}$  is shallow sandstone groundwater, and  $D_{\text{gw}}$  is deep dolomite groundwater.

## 4. Discussion

### 4.1. Seasonal Shifts in Water Flow Paths

Several lines of evidence point to the occurrence of a hydrological disconnection and a shift in dominant flow paths between the wet and dry seasons. First, our river stable isotope time-series data revealed a seasonal turning point during flow recession, from increasingly evaporated waters likely originating from wetland and floodplain drainage to more depleted waters that are representative of the dolostone aquifer (see change in arrow slopes in Figure 2b). According to our Bayesian source water mixing analyses, water sources to the river similarly transitioned from a dominance of shallow (i.e., transiting through laterite and sandstone) groundwater, wetland drainage and rainfall during the wet season and flow recession, to almost exclusively deep groundwater source during the dry season (Figure 4).

**Table 2**  
Seasonal and Annual DIC Flux Estimates According to Two Different Bayesian Source Mixing Scenarios

Bayesian mixing	Period	Biogenic DIC ( $\text{Mg C km}^{-2} \text{ yr}^{-1}$ )	Geogenic DIC ( $\text{Mg C km}^{-2} \text{ yr}^{-1}$ )
Water tracers	Wet	18.7 [15.9, 21.9]–12.7 [10.9, 14.8]	0.9 [0.5, 1.4]–0.1 [0.1, 0.2]
	Recession	0.4 [0.3, 0.5]–0.2 [0.1, 0.2]	0.3 [0.2, 0.3]–0.0 [0.0, 0.0]
	Dry	0.1 [0.1, 0.1]–0.0 [0.0, 0.0]	0.1 [0.1, 0.1]–0.0 [0.0, 0.0]
	Total	19.3 [16.3, 22.6]–12.9 [10.9, 15.0]	1.3 [0.8, 1.8]–0.1 [0.1, 0.2]
C tracers	Wet	4.1 [2.7, 5.1]–3.1 [2.3, 3.8]	0.7 [0.3, 0.9]–0.1 [0.0, 0.1]
	Recession	0.4 [0.2, 0.5]–0.2 [0.1, 0.3]	0.1 [0.1, 0.2]–0.0 [0.0, 0.0]
	Dry	0.1 [0.1, 0.1]–0.0 [0.0, 0.0]	0.1 [0.1, 0.1]–0.0 [0.0, 0.0]
	Total	4.5 [3.0, 5.7]–3.3 [2.4, 4.0]	0.9 [0.4, 1.2]–0.1 [0.0, 0.1]

*Note.* The italicized values correspond to the fraction of DIC flux contributed by dissolved  $\text{CO}_2$ . Values in brackets correspond to the interquartile range of Bayesian simulations.

The source water age estimates offer additional evidence for this shift in dominant flow paths. Water sources tended to be relatively young (less than one year) during the wet period and recession, indicative of recent contributions from surface and shallow subsurface stores—although our data did not permit a clear distinction between wetland and subsurface sources. By contrast, waters collected under low-baseflow conditions originated from much older sources (>100 years), suggestive of the disconnection of all shallow flow paths carrying young waters and, as a result, the dominance of deep groundwater upwelling in the downstream reaches during the dry season. These results are consistent with an early conceptualisation of the catchment by Cook et al. (1998) and with recent tracer-aided hydrological modeling results (unpublished).

We also note that groundwaters from the shallow and deep aquifers were both more  $^{18}\text{O}$ -depleted than average precipitation, suggesting that more intense, depleted wet season precipitation events preferentially recharged the subsurface. This pattern is common in the tropics (Jasechko & Taylor, 2015; Sánchez-Murillo & Birkel, 2016) and in the monsoon-driven parts of Australia (Hollins et al., 2018), and here recharge may have occurred via the network of large macropores present in the shallow soil horizons (Cook et al., 1998; Doyle, 2001). Meanwhile, the lower than expected contribution of rainfall water (i.e., direct runoff) during the wet season (Figure 4a) may be explained by our averaging of 33 wet season samples, which would decrease the relative weighting of single (extreme) event responses to rainfall.

#### 4.2. Sources of DIC

Tropical savannas typically have a C3-C4 vegetation mixture (Bird et al., 1994; Lloyd et al., 2008), with the stable isotopic signature of soil  $\text{CO}_2$  in the range from  $-25$  to  $-19\text{‰}$  (unpublished data). These  $\delta^{13}\text{C}_{\text{CO}_2}$  signatures would result in  $\delta^{13}\text{C}_{\text{DIC}}$  signatures between  $-22$  and  $-16\text{‰}$ , after correcting for diffusion and dissolution effects. In the Howard River, the very  $^{13}\text{C}$  depleted  $\delta^{13}\text{C}_{\text{DIC}}$  values measured in shallow groundwater (mean  $-26.6\text{‰}$ ), and to a lower extent in wetland waters (mean  $-23.1\text{‰}$ ), suggest that the  $\text{CO}_2$  produced through the C3 photosynthetic pathway contributed more significantly than C4-derived  $\text{CO}_2$  to biogenic DIC. This may be an indication that savanna woodland and its associated root respiration and organic matter decomposition dominated the shallow groundwater biogenic C pool, and that lateral DIC transport occurred from shallow groundwater underlying savanna soils to wetlands. By contrast, the  $-15.5\text{‰}$  signature of waters contained in the dolostone aquifer is characteristic of a more  $^{13}\text{C}$ -enriched, carbonate mineral source (with a mean dolostone signature of  $-3.4\text{‰}$ ), for which the dissolving  $\text{CO}_2$  would be highly  $^{13}\text{C}$ -depleted, that is, C3-derived.

According to Keeling and Miller-Tans analyses, the sources of DIC to the river varied significantly from the wet to the dry season, from depleted to enriched  $\delta^{13}\text{C}_{\text{DIC}}$  signatures (Table 1). We interpret these results as the likely evolution of DIC sources from biogenic, respiration-derived, and typical of a savanna-dominated signal during the wet season, to geogenic, weathering-derived during the dry season. In a similar study, Bouillon et al. (2014) observed even more pronounced seasonal shifts in DIC between a biogenic and a geogenic end-member in a savanna-covered catchment of the Congo basin, suggesting that such seasonal changes may be a characteristic feature of the wet-dry tropics.

Nevertheless, we recognize that other processes that we did not explicitly measure may have affected the  $\delta^{13}\text{C}_{\text{DIC}}$  signatures observed in river samples. First, while in-stream photosynthesis can enrich  $\delta^{13}\text{C}_{\text{DIC}}$  in river networks (Parker et al., 2005), we hypothesize that river metabolism was negligible as a source and as a process affecting  $\delta^{13}\text{C}_{\text{DIC}}$ , given that most rivers in the region are nutrient-limited systems with relatively low metabolism (García et al., 2015; Townsend et al., 2011). Second, Rayleigh distillation processes related to microbial methanogenesis likely occurred within wetlands during the wet season, potentially enriching the riverine  $\delta^{13}\text{C}_{\text{DIC}}$  downstream. Elevated methane evasion fluxes were measured in seasonal wetlands near the Howard River (Bass et al., 2014; Beringer et al., 2013), a sign of strong methanogenic activity. Methanogenesis alone might explain the  $\sim+3\text{‰}$  enrichment observed between the shallow groundwater and wetlands.

Third, the process of  $\text{CO}_2$  evasion is known to cause fractionation of riverine  $\delta^{13}\text{C}_{\text{DIC}}$  (Doctor et al., 2008; Shin et al., 2011). Duvert, Bossa, et al. (2019) showed a strong longitudinal enrichment from  $-25.5$  to  $-19.6\text{‰}$  along the upstream reaches of the Howard River, where only biogenic DIC sources were expected, which was attributed to the sole effect of  $\text{CO}_2$  evasion. In our study, evasion may have shifted all river  $\delta^{13}\text{C}_{\text{DIC}}$  values upward (i.e., toward more enriched isotopic signatures), particularly in the wet season due to higher

turbulence in the river, but also in the dry season as suggested by the more enriched values in the river (mean  $-14.0\text{‰}$ ) compared to those in the contributing end-member (dolostone aquifer;  $-15.5\text{‰}$ ). Below, we further discuss the potential effects of  $\text{CO}_2$  evasion on our Bayesian source water mixing estimates, and how this potential bias was circumvented in our DIC flux calculations.

### 4.3. Hydrological Connectivity Controls Riverine DIC Composition

Senar et al. (2018) demonstrated the role of hydrological connectivity in controlling the magnitude and partitioning of catchment C fluxes. In their boreal catchment, high connectivity enhanced fluvial C export, while low connectivity resulted in higher rates of  $\text{CO}_2$  evasion from wetlands (Senar et al., 2018). Here the general agreement between our Bayesian source contribution analyses based on water versus DIC tracers also suggests that hydrological connectivity and dominant water flow paths controlled the composition and rate of DIC delivery to the river. During the wet season and flow recession, the temporary water stores within floodplains and wetlands were particularly important in contributing biogenic DIC to the river. The likely role of flooded land in fuelling fluvial C export to the Howard River is in line with recent work carried out in the Amazon and African tropics (Abril et al., 2014; Borges et al., 2015; Geeraert et al., 2017). In this study, we have not directly measured atmospheric exchange from seasonal wetlands, but we would also expect important  $\text{CO}_2$  fluxes to the atmosphere during the wet season (e.g., Beringer et al., 2013).

Once these landscape units became depleted or simply disconnected from the drainage network, the upstream reaches of the Howard River rapidly ceased to flow. As water sources were transitioning from a dominance of relatively young (less than one year) waters to almost exclusively deep groundwater, riverine DIC likewise switched to a mostly geogenic origin, contributed by dolostone weathering and carried by these much older water sources. High DIC concentrations under baseflow conditions have often been associated with a predominance of groundwater carrying carbonate weathering products (e.g., Atkins et al., 2017; Bouillon et al., 2014; Mann et al., 2014; Shih et al., 2018), although the origin of this groundwater-derived DIC has not always been clarified. Here we can establish with confidence that virtually all the dry-season DIC was geogenic—although technically, and as discussed above, a mixture of equal proportions of biogenic and geogenic C.

One exception to the consistent results between our water and C tracer partitioning analyses is the large input of shallow groundwater during the wet season (63% of the estimated water flux), which did not correspond to a large DIC contribution (5% of the estimated DIC flux; Figure 4). We suggest that this discrepancy results from the combination of two factors. First, the effect of  $\text{CO}_2$  evasion upon groundwater emergence likely resulted in enriched  $\delta^{13}\text{C}_{\text{DIC}}$  values in the river relative to shallow groundwater, thereby causing a potential underestimation of the shallow groundwater contribution to the DIC flux in the mixing analysis. We would indeed expect large proportions of DIC being delivered to the Howard River via shallow flow paths, as  $p\text{CO}_2$  within the shallow aquifer was  $>40,000$  ppm on average (Rudge, 2015), and generally, the role of subsurface waters as carrier of biogenic C is increasingly recognised in the tropics (Duvert et al., 2018; Johnson et al., 2008; Oviedo-Vargas et al., 2015).

Second, differentiating between water and solutes originating from shallow groundwater to those originating from wetlands proved particularly difficult. We would expect the shallow groundwater across the catchment to be tightly connected to seasonal wetlands, whether geographically isolated or not (Ameli & Creed, 2017), and for shallow flow paths draining the savanna woodland to feed those wetlands via lateral transport before eventually reaching the river network. These coupling mechanisms between shallow groundwater and wetlands may have resulted in some degree of overlap between the two sources, and to a potential underestimation of the wetland-derived water flux under wet conditions. Likewise, and as discussed above, the wetland DIC contributions may also encompass lateral transport of shallow groundwater carrying biogenic DIC produced within the root zone of savanna vegetation.

### 4.4. Biogenic Versus Geogenic DIC and Implications for C Accounting

Central to the notion of C accounting is the capacity of terrestrial ecosystems to sequester and store atmospheric  $\text{CO}_2$ . Because some of the biogenic C stored in ecosystems is lost to inland waters (Cole et al., 2007), potentially representing a significant loss to inferred soil C storage (Butman et al., 2016; Kling et al., 1991), it is important to account for such fluvial C losses in regional and global C budgets. In areas where ecosystems are underlain by carbonate rocks, estimating terrestrial C loss to rivers is complicated

by the co-occurrence of geogenic, weathering products in fluvial DIC. In this context, methods are needed that can single out the proportion of fluvial C that is of biogenic origin (e.g., Campeau et al., 2017; Horgby et al., 2019).

Here we found that the DIC derived from soil respiration contributed a much larger proportion (83–94%) to the total DIC flux than geogenic DIC (Table 2). The bulk of both biogenic and geogenic DIC was exported during the wet season, because of disproportionately high flow rates during that period, whereas the purely geogenic DIC flux observed during the dry season did not comparatively yield substantial fluxes. While the geogenic flux represented a small percentage of the total DIC export to the Howard River, it is likely that geogenic DIC would be much more prevalent in other settings. For instance, in areas where primary productivity is not as elevated as in the tropics, one would expect lower biogenic DIC export, hence a higher relative contribution of geogenic DIC (e.g., Shin et al., 2011; Telmer & Veizer, 1999). High-gradient catchments with potentially high weathering rates and readily available carbonate rocks have also shown to export predominantly geogenic DIC (Horgby et al., 2019).

Our calculations allowed us to derive an estimate of the magnitude of catchment-wide CO<sub>2</sub> evasion. We consider that our DIC flux estimates based on Bayesian source partitioning and water source tracers (EC and δ<sup>18</sup>O) represent more realistic fluxes than those based on C source tracers, because unlike δ<sup>13</sup>C<sub>DIC</sub>, the water tracers we used were conservative and not subject to CO<sub>2</sub> evasion effects. In other words, the ~+15-Mg C km<sup>-2</sup> yr<sup>-1</sup> discrepancy between our two annual biogenic DIC flux estimates is likely to reflect the amount of DIC that was lost to the atmosphere as groundwater entered wetlands and/or the river (Table 2). This hypothesis is supported by the consistent difference between the two CO<sub>2</sub> flux estimates (~+10 Mg C km<sup>-2</sup> yr<sup>-1</sup>), suggesting that only an exchange of CO<sub>2</sub> can be responsible for the observed gap. Using a combination of water and C tracers, we were therefore able to indirectly constrain the C pathway to the atmosphere.

Duvert, Bossa, et al. (2019) calculated an evasion flux for the Howard River of <1 Mg C km<sup>-2</sup> yr<sup>-1</sup>, much lower than our estimate here. However, we note that their value was not meant to reflect year-round conditions as it was based on baseflow measurements only, when wetland drainage was low and low turbulence may have resulted in low CO<sub>2</sub> evasion. Our refined estimate indicates that the evasion of biogenic CO<sub>2</sub> in the Howard River was likely double that of downstream biogenic DIC export, which outlines the significance of this flux and the importance of better quantifying CO<sub>2</sub> evasion in the wet-dry tropics.

## 5. Conclusions

Using multiple tracer data over two annual cycles in a catchment of the wet-dry tropics of Australia, we showed that the marked rainfall seasonality in the region drove consistent changes in the dominant flow paths to the river. Surface and shallow subsurface stores, including seasonally flooded land, discharged into the river during the wet season and flow recession, whereas streamflow was dominated by deep groundwater upwelling during the dry season. We also showed that these extreme hydrological changes resulted in changes to the sources of DIC, with alternating biogenic and geogenic DIC entering the river. Though important to maintain baseflow during the dry season, the flow-weighted geogenic contribution was minor on an annual basis (6–17%).

Our analyses also confirmed the significance of CO<sub>2</sub> evasion in this seasonal, flood-driven system. We consider that evasion occurred via the drainage of shallow groundwater carrying soil-respired CO<sub>2</sub> into flooded land, where evasion was facilitated because of long residence times and large surface area. Obtaining a more complete picture of the fluvial C flux in the Howard River will require better quantification of this evasion term, but also of other C forms that transit through the river, including DOC and particulate organic carbon.

Because systems of the wet-dry tropics are highly dynamic, more detailed, high-resolution measurements are required to clarify the intricate mechanisms that connect savannas, wetlands, shallow waters, and rivers during the active months of the wet season. In particular, future research should focus on better integrating wetland functioning into river models (Abril & Borges, 2019), a key component in the lowland wet-dry tropics. Also needed is the incorporation of DIC data, and of the processes driving DIC transport, into coupled hydro-biogeochemical models.

## Acknowledgments

All the data underlying the findings of this article can be accessed in the Hydroshare repository at <https://www.hydroshare.org/resource/c15902a78ff34e2f8a88458805065d75>. This work was supported by an ARC Discovery grant (DP160101497) and an ANSTO research grant (11066). C.B. was funded by a CDU Visiting Scholar grant. Our thanks go to the Northern Territory Government for access to site, and particularly to Melissa Woltmann, Steven Tickell, and Roger Farrow for sharing data and general support. Several colleagues assisted with fieldwork, technical support (Matthew Northwood, Mylène Bossa, Diego Alvarez, and Michael Stauder), and lab work (Dionisia Lambrinidis, Alea Rose, and Robert Chisari).

## References

- Abbott, B. W., Baranov, V., Mendoza-Lera, C., Nikolakopoulou, M., Harjung, A., Kolbe, T., et al. (2016). Using multi-tracer inference to move beyond single-catchment ecohydrology. *Earth-Science Reviews*, *160*, 19–42.
- Abril, G., & Borges, A. V. (2019). Ideas and perspectives: Carbon leaks from flooded land: do we need to replumb the inland water active pipe? *Biogeosciences*, *16*, 769–784.
- Abril, G., Martinez, J.-M., Artigas, L. F., Moreira-Turcq, P., Benedetti, M. F., Vidal, L., et al. (2014). Amazon River carbon dioxide outgassing fuelled by wetlands. *Nature*, *505*(7483), 395–398. <https://doi.org/10.1038/nature12797>
- Ameli, A. A., & Creed, I. F. (2017). Quantifying hydrologic connectivity of wetlands to surface water systems. *Hydrology and Earth System Sciences*, *21*, 1791–1808.
- Atkins, M. L., Santos, I. R., & Maher, D. T. (2017). Seasonal exports and drivers of dissolved inorganic and organic carbon, carbon dioxide, methane and  $\delta^{13}\text{C}$  signatures in a subtropical river network. *Science of The Total Environment*, *575*, 545–563. <https://doi.org/10.1016/j.scitotenv.2016.09.020>
- Bass, A. M., Bird, M. I., Munksgaard, N. C., & Wurster, C. M. (2012). ISO-CADICA: Isotopic-continuous, automated dissolved inorganic carbon analyser. *Rapid Communications in Mass Spectrometry*, *26*, 639–644.
- Bass, A. M., O'Grady, D., Leblanc, M., Tweed, S., Nelson, P. N., & Bird, M. I. (2014). Carbon dioxide and methane emissions from a wet-dry tropical floodplain in Northern Australia. *Wetlands*, *34*, 619–627.
- Beringer, J., Livesley, S. J., Randle, J., & Hutley, L. B. (2013). Carbon dioxide fluxes dominate the greenhouse gas exchanges of a seasonal wetland in the wet-dry tropics of northern Australia. *Agricultural and Forest Meteorology*, *182–183*, 239–247.
- Bird, M. I., Giresse, P., & Chivas, A. R. (1994). Effect of forest and savanna vegetation on the carbon-isotope composition of sediments from the Sanaga River, Cameroon. *Limnology and Oceanography*, *39*, 1845–1854.
- Birkel, C., Broder, T., & Biester, H. (2017). Nonlinear and threshold-dominated runoff generation controls DOC export in a small peat catchment. *Journal of Geophysical Research: Biogeosciences*, *122*, 498–513.
- Borges, A. V., Darchambeau, F., Teodoru, C. R., Marwick, T. R., Tamooh, F., Geeraert, N., et al. (2015). Globally significant greenhouse-gas emissions from African inland waters. *Nature Geoscience*, *8*, 637.
- Bouillon, S., Yambélé, A., Gillikin, D. P., Teodoru, C., Darchambeau, F., Lambert, T., & Borges, A. V. (2014). Contrasting biogeochemical characteristics of the Oubangui River and tributaries (Congo River basin). *Scientific Reports*, *4*, 5402.
- Boyer, E. W., Hornberger, G. M., Bencala, K. E., & McKnight, D. M. (1997). Response characteristics of DOC flushing in an alpine catchment. *Hydrological Processes*, *11*, 1635–1647.
- Butman, D., Stackpoole, S., Stets, E., McDonald, C. P., Clow, D. W., & Striegl, R. G. (2016). Aquatic carbon cycling in the conterminous United States and implications for terrestrial carbon accounting. *Proceedings of the National Academy of Sciences*, *113*, 58–63.
- Campeau, A., Bishop, K., Nilsson, M. B., Klemetsson, L., Laudon, H., Leith, F. I., et al. (2018). Stable carbon isotopes reveal soil-stream DIC linkages in contrasting headwater catchments. *Journal of Geophysical Research: Biogeosciences*, *123*, 149–167.
- Campeau, A., Wallin, M. B., Giesler, R., Löfgren, S., Mörth, C.-M., Schiff, S., et al. (2017). Multiple sources and sinks of dissolved inorganic carbon across Swedish streams, refocusing the lens of stable C isotopes. *Scientific Reports*, *7*, 9158.
- Cole, J. J., Prairie, Y. T., Caraco, N. F., McDowell, W. H., Tranvik, L. J., Striegl, R. G., et al. (2007). Plumbing the global carbon cycle: Integrating inland waters into the terrestrial carbon budget. *Ecosystems*, *10*, 172–185.
- Cook, P. G., Hatton, T. J., Pidsley, D., Herczeg, A. L., Held, A., O'Grady, A., & Eamus, D. (1998). Water balance of a tropical woodland ecosystem, Northern Australia: A combination of micro-meteorological, soil physical and groundwater chemical approaches. *Journal of Hydrology*, *210*, 161–177.
- Dick, J. J., Tetzlaff, D., Birkel, C., & Soulsby, C. (2015). Modelling landscape controls on dissolved organic carbon sources and fluxes to streams. *Biogeochemistry*, *122*, 361–374.
- Doctor, D. H., Kendall, C., Sebestyen, S. D., Shanley, J. B., Ohte, N., & Boyer, E. W. (2008). Carbon isotope fractionation of dissolved inorganic carbon (DIC) due to outgassing of carbon dioxide from a headwater stream. *Hydrological Processes*, *22*, 2410–2423.
- Doyle, N. (2001). *Extractive minerals within the outer Darwin area*. Darwin, NT: Northern Territory Geological Survey.
- Duvert, C., Alvarez, D., Bird, M., Bossa, M., Northwood, M., Rudge, M., et al. (2019). Data for dissolved carbon study in the Howard River, NT, Australia. HydroShare, <http://www.hydroshare.org/resource/c15902a78ff34e2f8a88458805065d75>
- Duvert, C., Bossa, M., Tyler, K. J., Wynn, J. G., Munksgaard, N. C., Bird, M. I., et al. (2019). Groundwater-derived DIC and carbonate buffering enhance fluvial  $\text{CO}_2$  evasion in two Australian tropical rivers. *Journal of Geophysical Research: Biogeosciences*, *124*, 312–327.
- Duvert, C., Butman, D. E., Marx, A., Ribolzi, O., & Hutley, L. B. (2018).  $\text{CO}_2$  evasion along streams driven by groundwater inputs and geomorphic controls. *Nature Geoscience*, *11*, 813–818.
- Duvert, C., Stewart, M. K., Cendón, D. I., & Raiber, M. (2016). Time series of tritium, stable isotopes and chloride reveal short-term variations in groundwater contribution to a stream. *Hydrology & Earth System Sciences*, *20*, 257–277.
- Fiebig, D. M., Lock, M. A., & Neal, C. (1990). Soil water in the riparian zone as a source of carbon for a headwater stream. *Journal of Hydrology*, *116*, 217–237.
- Garcia, E. A., Pettit, N. E., Warfe, D. M., Davies, P. M., Kyne, P. M., Novak, P., & Douglas, M. M. (2015). Temporal variation in benthic primary production in streams of the Australian wet-dry tropics. *Hydrobiologia*, *760*, 43–55.
- Geeraert, N., Omengo, F. O., Borges, A. V., Govers, G., & Bouillon, S. (2017). Shifts in the carbon dynamics in a tropical lowland river system (Tana River, Kenya) during flooded and non-flooded conditions. *Biogeochemistry*, *132*, 141–163.
- Hollins, S. E., Hughes, C. E., Crawford, J., Cendón, D. I., & Meredith, K. T. (2018). Rainfall isotope variations over the Australian continent: Implications for hydrology and isoscape applications. *Science of The Total Environment*, *645*, 630–645.
- Horgby, Å., Boix Canadell, M., Ulseth, A. J., Vennemann, T. W., & Battin, T. J. (2019). High-resolution spatial sampling identifies groundwater as driver of  $\text{CO}_2$  dynamics in an Alpine stream network. *Journal of Geophysical Research: Biogeosciences*, *124*, 1961–1976.
- Huang, T.-H., Fu, Y.-H., Pan, P.-Y., & Chen, C.-T. A. (2012). Fluvial carbon fluxes in tropical rivers. *Current Opinion in Environmental Sustainability*, *4*, 162–169.
- Jasechko, S., & Taylor, R. G. (2015). Intensive rainfall recharges tropical groundwaters. *Environmental Research Letters*, *10*, 124015.
- Johnson, M. S., Lehmann, J., Riha, S. J., Krusche, A. V., Richey, J. E., Ometto, J. P. H. B., & Couto, E. G. (2008).  $\text{CO}_2$  efflux from Amazonian headwater streams represents a significant fate for deep soil respiration. *Geophysical Research Letters*, *35*, L17401.
- Johnson, M. S., Weiler, M., Couto, E. G., Riha, S. J., & Lehmann, J. (2007). Storm pulses of dissolved  $\text{CO}_2$  in a forested headwater Amazonian stream explored using hydrograph separation. *Water Resources Research*, *43*, W11201.
- Keeling, C. D. (1958). The concentration and isotopic abundances of atmospheric carbon dioxide in rural areas. *Geochimica et Cosmochimica Acta*, *13*, 322–334.

- Kirchner, J. W., Feng, X., & Neal, C. (2000). Fractal stream chemistry and its implications for contaminant transport in catchments. *Nature*, 403(6769), 524–527. <https://doi.org/10.1038/35000537>
- Kling, G. W., Kipphut, G. W., & Miller, M. C. (1991). Arctic lakes and streams as gas conduits to the atmosphere: implications for tundra carbon budgets. *Science*, 251(4991), 298–301. <https://doi.org/10.1126/science.251.4991.298>
- Laudon, H., Berggren, M., Ågren, A., Buffam, I., Bishop, K., Grabs, T., et al. (2011). Patterns and dynamics of dissolved organic carbon (DOC) in boreal streams: The role of processes, connectivity, and scaling. *Ecosystems*, 14, 880–893.
- Lloyd, J., Bird, M. I., Vellen, L., Miranda, A. C., Veenendaal, E. M., Djagbletey, G., et al. (2008). Contributions of woody and herbaceous vegetation to tropical savanna ecosystem productivity: A quasi-global estimate. *Tree Physiology*, 28(3), 451–468. <https://doi.org/10.1093/treephys/28.3.451>
- Małozewski, P., & Zuber, A. (1982). Determining the turnover time of groundwater systems with the aid of environmental tracers: 1. Models and their applicability. *Journal of Hydrology*, 57, 207–231.
- Mann, P. J., Spencer, R. G. M., Dinga, B. J., Poulsen, J. R., Hernes, P. J., Fiske, G., et al. (2014). The biogeochemistry of carbon across a gradient of streams and rivers within the Congo Basin. *Journal of Geophysical Research: Biogeosciences*, 119, 687–702.
- Miller, J. B., & Tans, P. P. (2003). Calculating isotopic fractionation from atmospheric measurements at various scales. *Tellus B*, 55, 207–214.
- Munksgaard, N. C., Wurster, C. M., & Bird, M. I. (2011). Continuous analysis of  $\delta^{18}\text{O}$  and  $\delta\text{D}$  values of water by diffusion sampling cavity ring-down spectrometry: A novel sampling device for unattended field monitoring of precipitation, ground and surface waters. *Rapid Communications in Mass Spectrometry*, 25, 3706–3712.
- Öquist, M. G., Wallin, M., Seibert, J., Bishop, K., & Laudon, H. (2009). Dissolved inorganic carbon export across the soil/stream interface and its fate in a boreal headwater stream. *Environmental Science & Technology*, 43(19), 7364–7369. <https://doi.org/10.1021/es900416h>
- Oviedo-Vargas, D., Genereux, D. P., Dierick, D., & Oberbauer, S. F. (2015). The effect of regional groundwater on carbon dioxide and methane emissions from a lowland rainforest stream in Costa Rica. *Journal of Geophysical Research: Biogeosciences*, 120, 2579–2595.
- Parker, S. R., Poulson, S. R., Gammons, C. H., & DeGrandpre, M. D. (2005). Biogeochemical controls on diel cycling of stable isotopes of dissolved  $\text{O}_2$  and dissolved inorganic carbon in the Big Hole River, Montana. *Environmental Science & Technology*, 39(18), 7134–7140. <https://doi.org/10.1021/es0505595>
- Parnell, A. C., Phillips, D. L., Bearhop, S., Semmens, B. X., Ward, E. J., Moore, J. W., et al. (2013). Bayesian stable isotope mixing models. *Environmetrics*, 24, 387–399.
- Peel, M. C., Finlayson, B. L., & McMahon, T. A. (2007). Updated world map of the Köppen-Geiger climate classification. *Hydrology and Earth System Sciences*, 11, 1633–1644.
- R Core Team (2018). *R: A language and environment for statistical computing*. Vienna, Austria: R Foundation for Statistical Computing. <https://www.R-project.org/>
- Rudge, M. (2015). Tree increment and fluvial export as carbon sink pathways in high rainfall savanna of north Australia. *Honours Thesis, Charles Darwin University, Australia*.
- Sánchez-Murillo, R., & Birkel, C. (2016). Groundwater recharge mechanisms inferred from isoscapes in a complex tropical mountainous region. *Geophysical Research Letters*, 43, 5060–5069.
- Sawakuchi, H. O., Neu, V., Ward, N. D., Barros, M. L. C., Valerio, A. M., Gagne-Maynard, W., et al. (2017). Carbon dioxide emissions along the Lower Amazon River. *Frontiers in Marine Science*, 4, 76.
- Senar, O. E., Webster, K. L., & Creed, I. F. (2018). Catchment-scale shifts in the magnitude and partitioning of carbon export in response to changing hydrologic connectivity in a northern hardwood forest. *Journal of Geophysical Research: Biogeosciences*, 123, 2337–2352.
- Shih, Y. T., Chen, P. H., Lee, L. C., Liao, C. S., Jien, S. H., Shiah, F. K., et al. (2018). Dynamic responses of DOC and DIC transport to different flow regimes in a subtropical small mountainous river. *Hydrology and Earth System Sciences*, 22, 6579–6590.
- Shin, W. J., Chung, G. S., Lee, D., & Lee, K. S. (2011). Dissolved inorganic carbon export from carbonate and silicate catchments estimated from carbonate chemistry and  $\text{d}^{13}\text{C}$ -DIC. *Hydrology and Earth System Sciences*, 15, 2551–2560.
- Stewart, M. K., & McDonnell, J. J. (1991). Modeling base flow soil water residence times from deuterium concentrations. *Water Resources Research*, 27, 2681–2693.
- Stewart, M. K., & Morgenstern, U. (2016). Importance of tritium-based transit times in hydrological systems. *Wiley Interdisciplinary Reviews: Water*, 3, 145–154.
- Stock, B. C., Semmens, B. X. (2016). MixSIAR GUI user manual. Version 3.1. <https://github.com/brianstock/MixSIAR>.
- Telmer, K., & Veizer, J. (1999). Carbon fluxes,  $\text{pCO}_2$  and substrate weathering in a large northern river basin, Canada: Carbon isotope perspectives. *Chemical Geology*, 159, 61–86.
- Teodoru, C. R., Nyoni, F. C., Borges, A. V., Darchambeau, F., Nyambe, I., & Bouillon, S. (2015). Dynamics of greenhouse gases ( $\text{CO}_2$ ,  $\text{CH}_4$ ,  $\text{N}_2\text{O}$ ) along the Zambezi River and major tributaries, and their importance in the riverine carbon budget. *Biogeosciences*, 12, 2431–2453.
- Townsend, S. A., Webster, I. T., & Schult, J. H. (2011). Metabolism in a groundwater-fed river system in the Australian wet/dry tropics: Tight coupling of photosynthesis and respiration. *Journal of the North American Benthological Society*, 30, 603–620.
- Tunaley, C., Tetzlaff, D., Lessels, J., & Soulsby, C. (2016). Linking high-frequency DOC dynamics to the age of connected water sources. *Water Resources Research*, 52, 5232–5247.
- Tweed, S., Leblanc, M., Bass, A., Harrington, G. A., Munksgaard, N., & Bird, M. I. (2016). Leaky savannas: the significance of lateral carbon fluxes in the seasonal tropics. *Hydrological Processes*, 30, 873–887.
- Violette, A., Riotte, J., Braun, J.-J., Oliva, P., Marechal, J.-C., Sekhar, M., et al. (2010). Formation and preservation of pedogenic carbonates in South India, links with paleo-monsoon and pedological conditions: Clues from Sr isotopes, U–Th series and REEs. *Geochimica et Cosmochimica Acta*, 74, 7059–7085.
- Waldron, S., Scott, E. M., & Soulsby, C. (2007). Stable isotope analysis reveals lower-order river dissolved inorganic carbon pools are highly dynamic. *Environmental Science & Technology*, 41(17), 6156–6162. <https://doi.org/10.1021/es0706089>
- Wallin, M., Buffam, I., Öquist, M., Laudon, H., & Bishop, K. (2010). Temporal and spatial variability of dissolved inorganic carbon in a boreal stream network: Concentrations and downstream fluxes. *Journal of Geophysical Research: Biogeosciences*, 115, G02014.
- Winterdahl, M., Wallin, M. B., Karlsen, R. H., Laudon, H., Öquist, M., & Lyon, S. W. (2016). Decoupling of carbon dioxide and dissolved organic carbon in boreal headwater streams. *Journal of Geophysical Research: Biogeosciences*, 121, 2630–2651.
- Zimmer, M. A., & McGlynn, B. L. (2018). Lateral, vertical, and longitudinal source area connectivity drive runoff and carbon export across watershed scales. *Water Resources Research*, 54, 1576–1598.